SCIENCE CHINA
Technological Sciences

• Article •

July 2017 Vol.60 No.7: 1050–1057
doi: 10.1007/s11431-016-9007-6

Shock relations in gases of heterogeneous thermodynamic properties

HU ZongMin[1,2], ZHOU Kai[1,2], PENG Jun[1,2], LI JinPing[1*] & JIANG ZongLin[1,2]

[1] *State Key Laboratory of High-temperature Gas Dynamics, Institute of Mechanics, Chinese Academy of Sciences, Beijing 100190, China;*
[2] *School of Engineering Science, University of Chinese Academy of Sciences, Beijing 100049, China*

Received September 21, 2016; accepted January 24, 2017; published online March 23, 2017

Shock relations usually found in literatures are derived theoretically under the assumption of homogeneous thermodynamic properties, i.e., constant ratio of specific heats, γ. However, high temperature effects post a strong shock wave may result in thermodynamic heterogeneities and failure to the original shock relations. In this paper, the shock relations are extended to take account of high-temperature effects. Comparison indicates that the present approach is more feasible than other analytical approaches to reflect the influence of γ heterogeneity on the post-shock parameters.

shock wave, imperfect gas, heterogeneous, theoretical solution

Citation: Hu Z M, Zhou K, Peng J, et al. Shock relations in gases of heterogeneous thermodynamic properties. Sci China Tech Sci, 2017, 60: 1050–1057, doi: 10.1007/s11431-016-9007-6

1 Introduction

Shock waves are common discontinuities in supersonic compressible flows. Real-gas or high-temperature effects may occur within the shock layer around a hypersonic vehicle flying at very high Mach numbers and cause deviation from the aerodynamic performance predicted in an ideal-gas environment. It was reported that the deflection angle of body flap required to trim the space shuttle obiter in flight became twice of the preflight prediction [1]. Subsequent research indicated that such a pitch-up anomaly was due to the real-gas effects occurring in the shock layer which induced an increment of pitching moment [2–4].

It has been a great challenge to duplicate the hypersonic flight conditions in a ground-based test facility by far. The primary difficulty is that the total temperature of the working gas required to generate a hypersonic test flow may be far beyond the material endurance of an existing test facility. In addition, the core flow size and its duration of an available hypersonic test facility are usually insufficient for force measurements of a hypersonic test model of meaningful scale. Therefore, real-gas effects can hardly be directly evaluated in a ground-based test facility. Approximate approaches had to be used in the study of real-gas effects on space shuttle models in which inert gases with different values of γ were used in wind tunnel experiments [3,5]. Recently, the development of high enthalpy shock tunnels seems to be inspiring, for the huge scales in test time and test section size [6] in the case of impulse type facilities. Direct experimental evaluation of real-gas effect becomes possible. The bow shock shape of a Mars entry vehicle model were investigated in a series of hypersonic test facilities including reflected-type shock tunnels and shock-expansion tunnels. For the moderate total enthalpy cases, the shock standoff distance measured in reflected-type shock tunnels was much larger than that measured in shock expansion tunnels or that predicted by computations. Uncertainties in the thermodynamic status of the freestream conditions in the reflected-type shock tunnels were assumed to be

*Corresponding author (email: lijinping@imech.ac.cn)

the key problem among others [7]. Park stressed the aforementioned uncertainty in the prediction of the shock standoff distance as one of the unsolved aerothermodynamic problems in hypersonic flow research [8].

Computational fluid dynamic (CFD) has been a promising means to study real-gas effects which may take into account of detailed thermal and chemical reaction models for high temperature flows [3,9]. However, the quantitative uncertainties arising from the thermo-chemical kinetic models are still a great challenge as it was pointed out more than two decades ago [10,11].

Besides CFD, analytical approach may give an intuitive prediction of high-temperature real-gas effects. Hirschel and Weiland [12] proposed a jumping γ method to approximate shock relations in real gases. It was stated that the above approach was recommended for hypersonic flows at extremely high Mach numbers instead of moderate ones. In the present work, the shock relations in general forms are derived to be applicable for an extended scope of hypersonic flight regime which includes flights at moderate Mach numbers. Comparison with the existing approaches is also conducted focusing on the influence of γ heterogeneity on the shock relations.

2 Enthalpy with γ heterogeneity

When a vehicle flies in the air at sufficiently high Mach numbers, strong shock waves will be generated around it, either attached or detached. It is well known that high temperature gas effects should be considered to predict the thermodynamic parameters of the real gas post the shock wave while the air ahead can be treated as calorically perfect gas. In this condition, the specific heat ratio ahead and post a shock wave are discontinuous, i.e., $\gamma_1 \neq \gamma_2$. Consequently, the specific heat at constant pressure, Cp, can be obtained in the following equations with the given specific heat ratio since both gases across the shock wave are thermal perfect:

$$\begin{cases} Cp_1 = \dfrac{\gamma_1}{\gamma_1 - 1} R_1, & T_1 < T\mathrm{c}, \\ Cp_2 = \dfrac{\gamma_2}{\gamma_2 - 1} R_2, & T_2 \geq T\mathrm{c}, \end{cases} \tag{1}$$

where T_1 and T_2 are the gas temperatures ahead and post the shock wave, while Tc is the characteristic temperature above which γ switch occurs.

The associated enthalpy can be derived from Cp for a thermal perfect gas, e.g.

$$h_1 = \int_0^{T_1} Cp_1 \,\mathrm{d}T = \frac{\gamma_1}{\gamma_1 - 1} R_1 T_1, \quad T_1 < T\mathrm{c}, \tag{2}$$

$$h_2 = \int_0^{T_c} Cp_1 \,\mathrm{d}T + \int_{T_c}^{T_2} Cp_2 \,\mathrm{d}T_2, \quad T_2 \geq T\mathrm{c}, \tag{3}$$

or

$$h_2 = \frac{\gamma_2}{\gamma_2 - 1} R_2 T_2 - \left(\frac{\gamma_2}{\gamma_2 - 1} R_2 - \frac{\gamma_1}{\gamma_1 - 1} R_1 \right) T\mathrm{c}, \tag{4}$$

where we introduce a characteristic enthalpy, Δh_c, to represent the second term on the right hand side of eq. (4), i.e., $\Delta h_c = \left(\dfrac{\gamma_2}{\gamma_2 - 1} R_2 - \dfrac{\gamma_1}{\gamma_1 - 1} R_1 \right) T\mathrm{c}$. The enthalpy variation with temperature is schematically depicted in Figure 1 for imperfect air where the characteristic temperature Tc is supposed to be 600 K. In the figure, labels "continuous h_2" and "discontinuous h_2" denote the enthalpy formulation with and without the term Δh_c, respectively. It can be seen from the curves that Δh_c does not vary with temperature. Therefore, $\Delta h_c \ll h_2$ and it can be neglected when $T_2 \gg T$c in the case of very strong shock waves primarily dealt by Hirschel and Weiland [12]. However, for a shock wave of moderate strength, Δh_c becomes comparable to h_2 and should not be ignored.

3 Shock relations

3.1 Normal shock relations

The conservation equations for mass, moment and energy for a normal shock wave can be written as

$$\rho_1 u_1 = \rho_2 u_2, \tag{5}$$

$$\rho_1 u_1^2 + p_1 = \rho_2 u_2^2 + p_2, \tag{6}$$

$$\frac{1}{2} u_1^2 + h_1 = \frac{1}{2} u_2^2 + h_2. \tag{7}$$

Substituting eqs. (2) and (4) and the equation of state, $p = \rho RT$, into eq. (7), we have

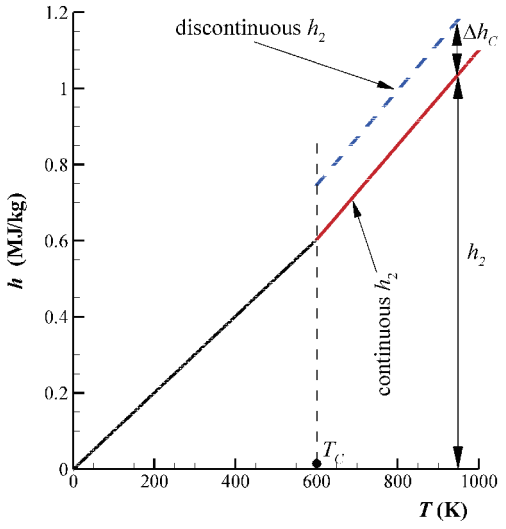

Figure 1 (Color online) Enthalpy models with γ heterogeneity induced by high-temperature (real-gas) effects.

$$\frac{1}{2}u_1^2+\frac{\gamma_1}{\gamma_1-1}\frac{p_1}{\rho_1}=\frac{1}{2}u_2^2+\frac{\gamma_2}{\gamma_2-1}\frac{p_2}{\rho_2}-\Delta h_c. \tag{8}$$

For a real gas under conditions of high pressure and low temperature, the state equation may be more complex to include intermolecular forces. In the current work, we only focus on the real-gas effects associated with high temperature. Therefore, the simple equation of state is still applicable.

From eqs. (5) and (6) we can get

$$u_1^2=\frac{\rho_2}{\rho_1}\frac{(p_2-p_1)}{(\rho_2-\rho_1)}, \tag{9}$$

$$u_2^2=\frac{\rho_1}{\rho_2}\frac{(p_2-p_1)}{(\rho_2-\rho_1)}. \tag{10}$$

Substituting eqs. (9) and (10) into eq. (8), we have the Rankine-Hugoniot (R-H) relation in a general form which can be written as

$$\frac{p_2}{p_1}=\frac{\left(\frac{\gamma_1+1}{\gamma_1-1}+2\Delta\tilde{h}_c\right)\frac{\rho_2}{\rho_1}-1}{\frac{\gamma_2+1}{\gamma_2-1}-\frac{\rho_2}{\rho_1}}, \tag{11}$$

where $\Delta\tilde{h}_c$ represents the dimensionless enthalpy difference and reads

$$\Delta\tilde{h}_c=\Delta h_c\frac{\rho_1}{p_1}=\left(\frac{\gamma_2}{\gamma_2-1}\frac{R_2}{R_1}-\frac{\gamma_1}{\gamma_1-1}\right)\frac{T\mathrm{c}}{T_1}, \tag{12}$$

it should be noted that $\Delta\tilde{h}_c$ is a model parameter which involves the characteristic temperature ratio, $T\mathrm{c}/T_1$.

Because that $\gamma_1=\gamma_2$, $R_1=R_2$ and $\Delta h_c=0$ hold across shock waves in a calorically perfect gas, the R-H relations as given in eq. (11) returns the original form as can be found in an aerodynamic textbook. Obviously, the original R-H relation only holds for shock waves which are not strong enough to incur vibration excitation and dissociation of polyatomic molecules and other thermo-chemical processes. For the situation of hypersonic flows in the presences of strong shock waves where the high-temperature effects are critical, eq. (11) shall be used.

The Mach number, M_1, the speed of sound, a_1, and the flow velocity, u_1, ahead of the shock wave hold the following relation:

$$u_1^2=M_1^2a_1^2=M_1^2\gamma_1\frac{p_1}{\rho_1}. \tag{13}$$

Substituting eq. (13) into eq. (9) yields the relation among the flow Mach number ahead of the shock wave and the pressure and density ratios

$$\frac{p_2}{p_1}=\frac{(\gamma_1M_1^2+1)\frac{\rho_2}{\rho_1}-\gamma_1M_1^2}{\rho_2/\rho_1}. \tag{14}$$

Combining eqs. (11) and (14), we obtain a quadratic equation about the unknown density ratio, ρ_2/ρ_1, across the normal shock wave

$$\left[\gamma_1M_1^2+\frac{2\gamma_1}{\gamma_1-1}+2\Delta\tilde{h}_c\right]\left(\frac{\rho_2}{\rho_1}\right)^2-\left[\frac{2\gamma_2}{\gamma_2-1}(\gamma_1M_1^2+1)\right]\frac{\rho_2}{\rho_1}+\left[\frac{\gamma_2+1}{\gamma_2-1}\gamma_1M_1^2\right]=0. \tag{15}$$

The solution to eq. (15) reads

$$\frac{\rho_2}{\rho_1}=\frac{\frac{\gamma_2}{\gamma_2-1}(\gamma_1M_1^2+1)+\frac{\sqrt{A}}{\gamma_2-1}}{\gamma_1M_1^2+\frac{2\gamma_1}{\gamma_1-1}+2\Delta\tilde{h}_c}, \tag{16}$$

where

$$A=(\gamma_1M_1^2)^2-2\left[\frac{\gamma_2^2-\gamma_1}{\gamma_1-1}+(\gamma_2^2-1)\Delta\tilde{h}_c\right]\gamma_1M_1^2+\gamma_2^2.$$

For a calorically perfect gas, $\gamma_1=\gamma_2$ and $R_1=R_2$, a compact form of the shock relation can be achieved which is unique to that given in an aerodynamic textbook for shock waves with homogeneous γ. Here, it is rewritten as

$$\left[\frac{\rho_2}{\rho_1}\right]_{\substack{\gamma_1=\gamma_2\\R_1=R_2}}=\frac{(\gamma+1)M_1^2}{(\gamma-1)M_1^2+2}. \tag{17}$$

We can obtain from the shock relation, eq. (16), as M_1 approaches ∞

$$\left[\frac{\rho_2}{\rho_1}\right]_{M_1\to\infty}=\frac{\gamma_2+1}{\gamma_2-1}, \tag{18}$$

it says that the maximum density ratio is only related to the specific heat ratio post an extremely strong shock wave when $M_1\to\infty$. Generally, high temperature effects may result in $\gamma_2<\gamma_1$, which indicates much more compressibility across a strong shock wave than that for a calorically prefect gas.

Once the density ratio ρ_2/ρ_1 is solved, it is easy to obtain the pressure ratio p_2/p_1using eq. (11) or (14). The temperature ratio T_2/T_1, the post shock Mach number $M_2$and other parameters can be deduced accordingly.

It should be noted that Hirschel and Weiland [12] use "discontinuous h_2" as depicted in Figure 1 for simplification. The consequential relations for a normal shock wave can be analogously obtained by setting $\Delta h_c=0$ or $\Delta\tilde{h}_c=0$ accordingly. Here, they are not repeated for concise. Such a simplification may incur considerable errors if applied for shock waves of moderate strength as can be seen in a comparative study in Section 3.

3.2 Oblique shock relations

An oblique shock wave is schematically shown in Figure 2,

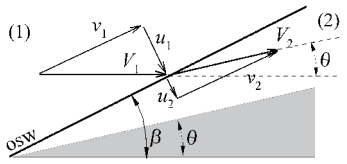

Figure 2 Schematic illustration of an oblique shock wave.

where β and θ denote the shock angle and flow deflection angle, respectively. It is known that the thermodynamic variable changes across an oblique shock wave are governed only by the normal velocity components since the tangential component keeps constant i.e., $v_1 = v_2$. The governing eqs. (5), (6) and (7) for a normal shock wave are still applicable for an oblique shock wave while u_1 and u_2 represent the velocity components normal to the shock front. In consequence, the Rankine-Hugoniot relation as given by eqs. (11), (9) and (10) still hold for an oblique shock wave.

The velocity components normal and tangential to the shock front, e.g., u_1, v_1, u_2 and v_2, as illustrated in Figure 2, hold the following geometric relations:

$$\begin{aligned} &u_1 = V_1\sin\beta, \quad v_1 = V_1\cos\beta, \\ &u_2 = V_2\sin(\beta-\theta), \quad v_2 = V_2\cos(\beta-\theta), \\ &v_2 = v_1. \end{aligned} \tag{19}$$

The above equations introduce β and θ into the oblique relations. Note that

$$u_1^2 = V_1^2\sin^2\beta = M_1^2a_1^2\sin^2\beta = M_1^2\gamma_1\frac{p_1}{\rho_1}\sin^2\beta. \tag{20}$$

Substituting eq. (20) into eq. (9) yields

$$\frac{p_2}{p_1} = \frac{(\gamma_1M_1^2\sin^2\beta+1)\dfrac{\rho_2}{\rho_1}-\gamma_1M_1^2\sin^2\beta}{\rho_2/\rho_1}. \tag{21}$$

Combining eq. (21) and the Rankine-Hugoniot relation as given in eq. (11) in Section 3.1, we can obtain a quadratic equation about unknown ρ_2/ρ_1 for an oblique shock wave analogously to that for a normal shock wave as given in eq. (15)

$$\begin{aligned} &\left[\gamma_1M_1^2\sin^2\beta+\frac{2\gamma_1}{\gamma_1-1}+2\Delta\tilde{h}_c\right]\left(\frac{\rho_2}{\rho_1}\right)^2 \\ &-\left[\frac{2\gamma_2}{\gamma_2-1}\left(\gamma_1M_1^2\sin^2\beta\right)+1\right]\frac{\rho_2}{\rho_1}+\left[\frac{\gamma_2+1}{\gamma_2-1}\gamma_1M_1^2\sin^2\beta\right] = 0. \end{aligned} \tag{22}$$

In eq. (22), the shock angle β is an unknown variable. From eqs. (19) and (5) we obtain

$$\frac{\tan\beta}{\tan(\beta-\theta)} = \frac{u_1v_2}{v_1u_2} = \frac{u_2}{u_1} = \frac{\rho_2}{\rho_1}, \tag{23}$$

or

$$\tan\theta\tan^2\beta+\left(1-\frac{\rho_2}{\rho_1}\right)\tan\beta+\frac{\rho_2}{\rho_1}\tan\theta = 0. \tag{24}$$

Since $\sin^2\beta = \tan^2\beta/(1+\tan^2\beta)$, eqs. (22) and (24) can be solved simultaneously to obtain ρ_2/ρ_1 and $\tan\beta$. Replacing M_1 with $M_{1n} = M_1\sin\beta$ in eq. (16) we get the final solution for the oblique shock relation, i.e.,

$$\frac{\rho_2}{\rho_1} = \frac{\dfrac{\gamma_2}{\gamma_2-1}(\gamma_1M_{1n}^2+1)+\dfrac{\sqrt{A_n}}{\gamma_2-1}}{\gamma_1M_{1n}^2+\dfrac{2\gamma_1}{\gamma_1-1}+2\Delta\tilde{h}_c}, \tag{25}$$

where

$$A_n = (\gamma_1M_{1n}^2)^2-2\left[\frac{\gamma_2^2-\gamma_1}{\gamma_1-1}+(\gamma_2^2-1)\Delta\tilde{h}_c\right]\gamma_1M_{1n}^2+\gamma_2^2.$$

Once ρ_2/ρ_1 is solved, other quantities such as β, p_2/p_1, and T_2/T_1 can be obtained accordingly. Letting $\Delta\tilde{h}_c = 0$ in eq. (25) we may have the oblique shock relations using "discontinuous h_2" as proposed by Hirschel and Weiland [12]. Furthermore, setting $\gamma_1 = \gamma_2$ and $R_1 = R_2$ for calorically perfect gases, we may achieve a compact form of oblique shock relations as given in any aerodynamic textbook.

4 Comparative study

The shock relations featuring heterogeneous γ developed in the preceding sections can reflect real-gas effects in imperfect gas flow. Hereinafter, we denote the current analytical approach as IP and compare it with other approaches to evaluate real-gas effects on shock waves of moderate strength. Under such situations, the vibration excitation shall cause a decrease of γ post the shock wave according to the air kinetic theory, i.e., $\gamma_2 < \gamma_1 = 1.4$. The simplified approach proposed by Hirschel and Weiland [12] is named SIP. In addition, the approximate approach in wind tunnel experiments [3,5] using inert gases is also considered in the following comparison. Since the test gases in such experiments are inert or calorically perfect, we denote the corresponding analytical solution as CP. In the coming subsections, normal shock waves and oblique shock waves are investigated successively for comparison in detail.

4.1 Normal shock wave

The flow temperature ahead the studied normal shock waves is chose according the atmosphere at the altitude of 30 km, i.e., T_1=226 K while the characteristic temperature for vibration excitation Tc=600 K is used to calculate $\Delta\tilde{h}_c$ for all the coming cases. Flow variable ratios across the normal shock waves, for instance, T_2/T_1, ρ_2/ρ_1 and p_2/p_1, are depicted respectively in Figure 3 for direct comparison. The dashed, solid and dash-dotted lines in each frame represent solutions

corresponding to IP, CP and SIP approaches, respectively. In each frame, the state when $\gamma_2 = 1.4$ corresponds to the calorically perfect condition under which real-gas effects don not occur in the air flow of interest.

Generally, vibration excitation may result in an increase in the density or pressure ratio across a normal shock wave but a decrease in the temperature ratio. As can been seen from Figure 3, all the aforementioned approaches succeed in simulating the overall trends of post-shock temperature and density. However, the CP approach [3,5], as shown by the solid line in either Figure 3(c) or (f), gives an opposite variation of pressure as compared with the else. This implies that using inert test gases with $\gamma < 1.4$ in a cool tunnel experiment may lead to a decrement of surface pressure at the nose of a hypersonic vehicle where a bow shock exists. It results in a nose-down moment which does not coincide with the findings of pitch-up anomaly [3,5]. More details will be given in the following sections.

A quantitative comparison among the relative changes of T_2/T_1, ρ_2/ρ_1 and p_2/p_1, with respect to the calorically perfect situation, i.e., $\gamma_2 = 1.4$ for air, is summarized in Table 1. On the whole, all the three approaches can successfully demonstrate less significant change to the pressure ratio p_2/p_1 than that to the temperature or density ratio. From differentiation of eq. (14) we have

$$\xi = \frac{d\left(\frac{p_2}{p_1}\right)/\frac{p_2}{p_1}}{d\left(\frac{\rho_2}{\rho_1}\right)/\frac{\rho_2}{\rho_1}} = \frac{1}{\left[1+(\gamma_1 M_1^2)^{-1}\right]\frac{\rho_2}{\rho_1}-1}. \tag{26}$$

As $\rho_2/\rho_1 \gg 1$ for strong shock waves in hypersonic flows, $\xi \ll 1$. Eq. (26) gives the reason why $\Delta p \ll \Delta\rho$ as demonstrated in Table 1. Such a conclusion keeps qualitatively no matter high-temperature effects are significant or not as γ_2 does not present in the right hand side of eq. (26). The CP approach, however, shows a much more decrease in temperature than IP approach. From above investigations, we can find that using inert test gases to simulate real-gas effects are not recommended when the stagnation heat flux or pressure is of interest.

Recalling that in the SIP approach [12] Δh_c (see Figure 1) is artificially added to the post-shock enthalpy, herein we may see the consequence in Figure 3 and Table 1. Such an energy injection results in much greater changes in T_2/T_1, ρ_2/ρ_1 and

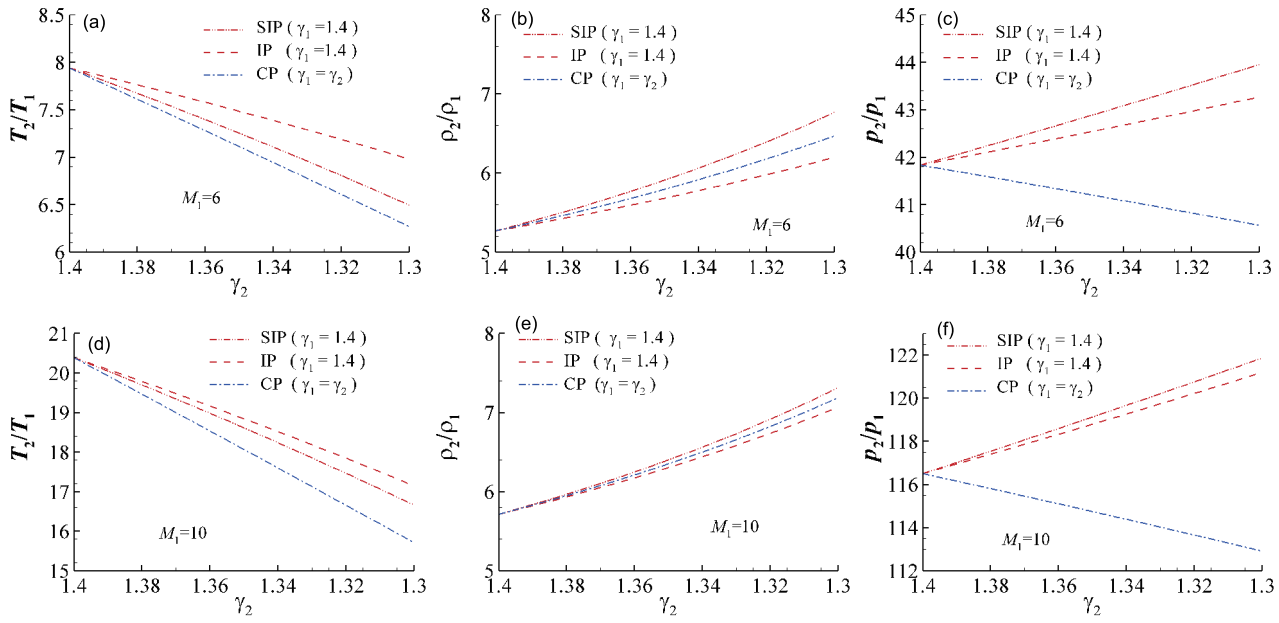

Figure 3 (Color online) Normal shock wave properties with varying γ_2, T_1=226 K, Tc=600 K. (a–c) M_1=6; (d–f) M_1=10.

Table 1 Relative changes of ρ_2/ρ_1, T_2/T_1 and p_2/p_1 when γ_2 approaching 1.3 for normal shock waves (γ_2=1.3 corresponding to the state at which the molecular vibration of oxygen and nitrogen is full excited)

M_1	$\Delta\rho_{IP}$	$\Delta\rho_{SIP}$	$\Delta\rho_{CP}$	ΔT_{IP}	ΔT_{SIP}	ΔT_{CP}	Δp_{IP}	Δp_{SIP}	Δp_{CP}
6	+17.6%	+29.0%	+22.7%	–11.4%	–17.7%	–20.6%	+3.4%	+5.1%	–3.0%
10	+23.9%	+28.2%	+26.1%	–15.7%	–18.1%	–23.0%	+4.0%	+4.6%	–3.1%
15	+25.7%	+27.8%	+26.8%	–17.2%	–18.3%	–23.6%	+4.2%	+4.5%	–3.1%

p_2/p_1 than the IP approach proposed in the present work, especially for the case with relatively low Mach number, e.g., $M_1 = 6$. As the Mach number increases, the discrepancy gets more and more insignificant which coincides to the fact concluded in Section 1 that Δh_c gets negligible when $T_2 \gg T$c for sufficiently strong shock waves. Carefully examining Δp_{SIP} in Table 1, we may find that it decreases as M_1 increases. Obviously, such a phenomenon does not reflect the nature of real-gas effects of hypersonic air flows. Based on the investigations, we recommend IP approach instead of SIP for hypersonic flows at moderate Mach numbers.

4.2 Oblique shock wave

The freestream flow conditions studied in Section 3.1 is used again for the study of oblique shock waves. Putting a wedge with a vertex angle of $\theta = 25°$ in the hypersonic flow, an oblique shock wave (OSW) attaching to the wedge may be generated as schematically shown in Figure 2. Hypersonic flows with $M_1 = 10$, 15 and 20 are respectively considered in the following analysis.

The oblique shock wave properties, T_2/T_1, ρ_2/ρ_1 and p_2/p_1 are comparatively depicted in Figure 4 and listed in Table 2. Unlike the CP approach failing to reflect real-gas effect on pressure across a normal shock wave, all approaches reproduce qualitatively consistent trends for an oblique shock wave. Briefly speaking, the heterogeneity of induced by high-temperature post an oblique shock wave leads to decreases both in the temperature and pressure ratios but an increase in the density ratio.

Examining the quantitative comparison in Table 2, we may find that the CP approach causes post-shock pressure decrease around three times more than the IP approach. In addition, it predicts much more decrease in temperature. Based on the aforementioned investigation, we may conclude that using inert test gases in wind tunnel experiments [3,5] to simulate the well known pitch-up anomaly induced by real-gas effects is not a reasonable option.

As compared with the IP approach, the over prediction by the SIP approach as respectively illustrated in Figure 4 or Table 2 is unacceptable for the $M_1 = 10$ case. The discrepancy tends to decrease as the Mach number increases. Furthermore, Δp_{SIP} as given in Table 2 decreases as M_1 increases indicating an illogic prediction. Therefore, the IP approach proposed in the present work is the best choice to simulate the high-temperature effects of hypersonic flows at moderate Mach numbers.

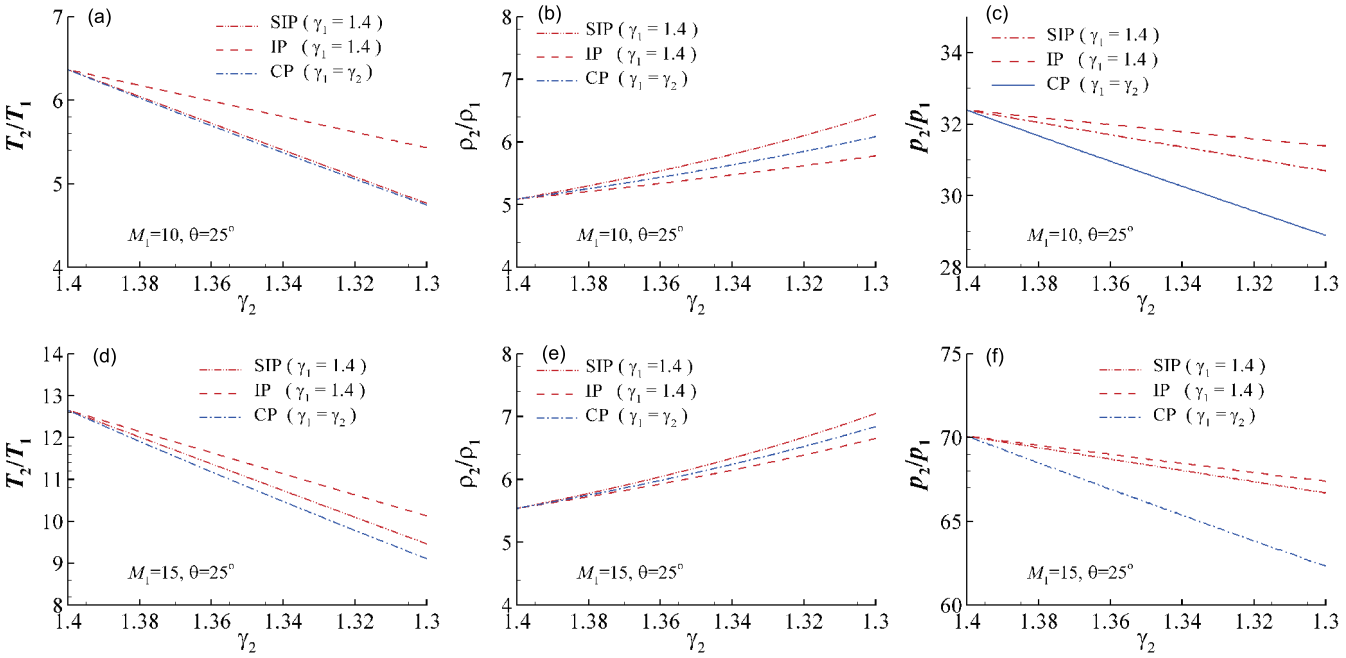

Figure 4 (Color online) Oblique shock wave properties with varying γ_2, T_1=226 K, Tc=600 K. (a–c) M_1=6; (d–f) M_1=10.

Table 2 Relative changes of ρ_2/ρ_1, T_2/T_1 and p_2/p_1 when γ_2 approaching 1.3 for oblique shock waves

M_1	$\Delta\rho_{IP}$	$\Delta\rho_{SIP}$	$\Delta\rho_{CP}$	ΔT_{IP}	ΔT_{SIP}	ΔT_{CP}	Δp_{IP}	Δp_{SIP}	Δp_{CP}
10	+13.5%	+26.5%	+19.5%	–14.7%	–25.1%	–25.4%	–3.1%	–5.2%	–10.8%
15	+20.0%	+27.1%	+23.3%	–19.9%	–25.1%	–27.9%	–3.8%	–4.8%	–11.0%
20	+23.0%	+27.3%	+25.1%	–22.1%	–25.2%	–29.0%	–4.1%	–4.7%	–11.2%

4.3 Discussion

During the first atmosphere re-entry, the space shuttle orbiter encountered a severe nose-up pitching moment increment relative to the pre-flight prediction [1]. Such a pitch-up anomaly aroused concerns among researchers especially those from NASA and ESA. Conventional hypersonic wind tunnel experiments in air convinced a discrepancy of center of pressure location, $\Delta\chi_{CP} = 20$ cm, from the flight data for $M_1 = 10$. The discrepancy was thought to be caused by the incapability of such kind of cool tunnel to simulate real-gas effects. Therefore, the facilities at Langley were used to simulate real-gas effects by using an inert test gas which has a lower γ than ideal air [5].

The shock polars for a hypersonic flow with $M_1 = 10$, $T_1 = 226$ K are combined in Figure 5 to compare the theoretical solutions corresponding to the aforementioned approaches. In each frame, CP ($\gamma_2 = \gamma_1 = 1.4$), CP ($\gamma_2 = \gamma_1 = 1.3$) and IP ($\gamma_2 = 1.3$, $\gamma_1 = 1.4$) denote the ideal air approach, inert gas approach [3,5] and heterogeneous approach proposed in the present work, respectively. A blunt-nosed hypersonic vehicle flying at M_1 with an angle of attack, α, is schematically depicted in Figure 5(c).

It can be seen from Figure 5(a) that the IP solution (dashed profile) demonstrates a pressure increment along the "strong branch" but a "pressure decrement" along the "weak branch" of the shock polar as compared with the CP solution (solid profile). As shown in Figure 5(c), the bow shock wave in the nose region corresponds to the "strong branch" while the oblique shock wave corresponds to the "weak branch". Based on the above investigations, the real-gas effects result in an increment of pitch-up moment which coincides with the flight data [1]. However, the inert test gas approach [3,5] as given by the dash-dotted profile in Figure 5(b) indicates a pressure decrease along both the "strong branch" and "weak branch". However, the overshot decrease of surface pressure (see Δp_{CP} in Table 2) along the "weak branch" may partially offset the opposite pressure variation along the "strong branch". Fortunately, the inert test gas approach is still capable of qualitatively simulate the so-called "pitch-up anomaly". Therefore, the approach using an inert test gas with γ lower than air in a "cool" tunnel [5] to simulate real-gas effects needs further confirmation. Jiang and Yu [13] mentioned a hypersonic shock tunnel which can simulate the total temperature of hypersonic flights. Such a "hot" tunnel may be a better choice to study real-gas effects than the conventional hypersonic wind tunnels.

It should be noted that the present shock solution is an approximate approach which treats the specific heat *Cp* as two different constants (see eq. (1)) ahead and post a shock wave, respectively. This leads to a piecewise linear function of enthalpy about temperature as depicted in Figure 1. It is well known that the specific heat for a high temperature gas is an exponential function about temperature derived from quantum mechanics (see the ref. [14]). Polynomial equations [15] are generally used in CFD for thermodynamic properties of species. However, we cannot get theoretical shock

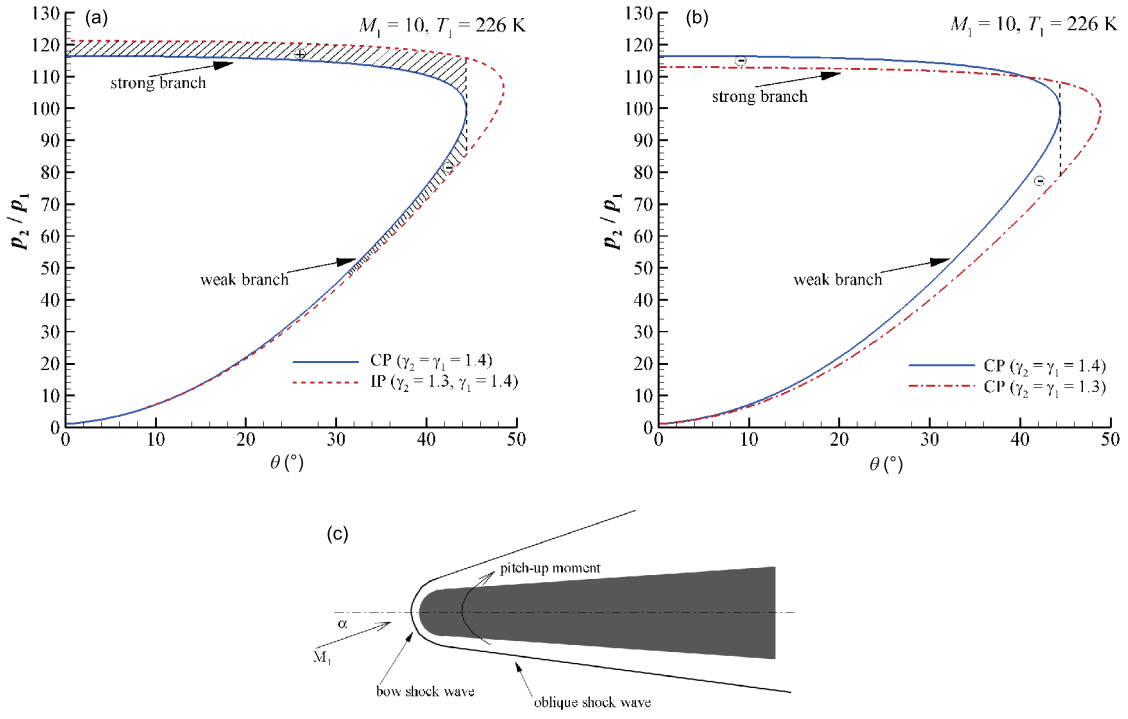

Figure 5 (Color online) Shock polar comparison (a), (b) and sketch of a blunt-nosed hypersonic vehicle (c) with a pitch-up moment.

solution in an explicit form as given in eq. (16) or (25) if these complex functions are used in the present work. In addition, the primary point of the present work focuses on shock waves of moderate strength and the shock relations in the presence of γ heterogeneity associated with vibration excitation. Therefore, the simplified models of thermodynamic properties are used in the present analytical solution. A comparison between the present enthalpy model with the Polynomial equation [15] for air is shown in Figure 6. It can be seen that the accuracy of the simplification is acceptable.

5 Conclusions

In the present work, the shock relations considering heterogeneous γ has been deduced to study high-temperature (real-gas) effects. The obtained normal and oblique shock relations encompass much more thermodynamic features of hypersonic real-gas flows than the existing analytical approaches. On the one hand, the new shock relations are derived from a continuous model of enthalpy associated with γ heterogeneity. Such an improvement can eliminate the error in the simplified approach [12] induced by the artificial energy addition to the post shock flow, i.e., Δh_c, especially for shock waves of moderate strength. On the other hand, the proposed shock relations reveal the pressure decrease along the weak branch of a shock polar and the pressure increase along the strong branch, respectively. Therefore, one can have relatively reliable preflight approximation of the aerodynamic force and moment of a hypersonic vehicle with a blunted nose. Comparative studies indicate that new shock relations work better than the other options for shock analysis in hypersonic flows especially at moderate Mach numbers.

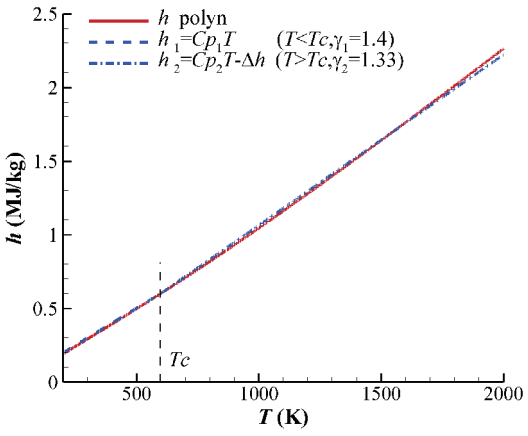

Figure 6 (Color online) Comparison between different enthalpy models of air.

The underlying mechanism associated with the "pitch-up anomaly" that a blunt-nosed vehicle encounters during its hypersonic flight can be clearly demonstrated by using the shock polar analysis based on the proposed shock relations. The pressure increases along the nose surface and decreases along the downstream surface which results in an increment of nose-up moment. The reported "cool" tunnel tests using an inert test gas with γ lower than ideal air cannot reflect such a real-gas mechanism completely. 'Hot' tunnel experiments are necessary and recommended to study real-gas effects for hypersonic aerodynamics in future.

This work was supported by the National Natural Science Foundation of China (Grant Nos. 11672308 and 11532014), and Innovation Grant of Chinese Academy of Sciences.

1 Woods W C, Arlington J P, Hamilton H H. A review of preflight estimates of real-gas effects on space shuttle aerodynamic characteristics. In: Proceedings of Orbiter Experiments Aerothermodynamics Symposium. Hampton: NASA, 1983. 309–346
2 Maus J R, Griffith B J, Szema K Y, et al. Hypersonic Mach number and real gas effects on space shuttle orbiteraerodynamics. J Spacecraft Rockets, 1984, 21: 136–141
3 Brauckmann G J, Paulson Jr. J W, Weilmuenster K J. Experimental and computational analysis of shuttle orbiter hypersonic trim anomaly. J Spacecraft Rockets, 1995, 32: 758–764
4 Bertin J J, Cummings R M. Critical hypersonic aerothermodynamic phenomena. Annu Rev Fluid Mech, 2006, 38: 129–157
5 Muylaert J, Walpot L, Rostand P, et al. Extrapolation from wind tunnel to flight: Shuttle orbiter aerodynamics. Technical Report. NASA, 1998
6 Holden M S, Wadhams T P, MacLean M, et al. Experimental studies in hypersonic flows for facility and code validation. AIAA Paper No. 2007-1304, 2007
7 Holden M S, Wadhams T P, MacLean M, et al. A review of basic research and development programs conducted in the LENS facilities in hypervelocity flows. AIAA Paper No. 2012-169, 2012
8 Park C. Hypersonic aerothermodynamics: Past, present and future. Int J Aeronaut Space Sci, 2013, 14: 1–10
9 Li K, Hu Z M, Jiang Z L. Numerical studies on the effect of the key parameter to hypersonic "pitch-up anomaly". Sci Sin-Phys Mech Astron, 2015, 45: 034701
10 Furudate M, Nonaka S, Sawada K. Behavior of two-temperature model in intermediate hypersonic regime. J Thermophys Heat Transfer, 1999, 13: 424–430
11 Tirsky G A. Up-to-date gasdynamic models of hypersonic aerodynamics and heat transfer with real gas properties. Ann Rev Fluid Mech, 1993, 25: 151–181
12 Hirschel E H, Weiland C. Selected Aerothermodynamic Design Problems of Hypersonic Flight Vehicles. Berlin: Springer-Verlag, 2009
13 Jiang Z L, Yu H R. Experiments and development of long test duration hypervelocity detonation-driven shock tunnel (LHDst). AIAA Paper No. 2014-1012, 2014
14 Anderson J D. Hypersonic and High Temperature Gas Dynamic. New York: McGraw-Hill, 1989
15 McBride B J, Zehe M J, Gordon S. NASA Glenn coefficients for calculating thermodynamic properties of individual species. Technical Report. NASA, 2002